2011

Effects of Mass Layer Nonuniformity on a Quartz-Crystal Microbalance

Nan Liu
University of Nebraska-Lincoln

Jiashi Yang
University of Nebraska-Lincoln

Weiqiu Chen
Zhejiang University, chenwq@zju.edu.cn

Effects of Mass Layer Nonuniformity on a Quartz-Crystal Microbalance

Nan Liu, Jiashi Yang, and Weiqiu Chen

***Abstract*—We study the effects of the nonuniform thickness of a thin mass layer on a quartz-crystal microbalance. A theoretical analysis is performed on thickness-shear (TSh) vibration of an AT-cut quartz plate with a nonuniform mass layer. Mindlin's 2-D equation for TSh vibration of a quartz plate is used. An elliptical mass layer with stepped thickness is considered which allows an exact analysis based on the plate equation. Free vibration frequencies and modes are obtained. The effects of the mass layer nonuniformity are examined. Results show that a mass layer thicker at the center tends to confine more modes under the mass layer and push the distribution of the TSh displacement toward the center.**

***Index Terms*—Mass layer, Mindlin's equation, quartz-crystal microbalance, thickness-shear vibration, vibration mode.**

I. Introduction

QUARTZ-CRYSTAL resonators (QCRs) operating with plate TSh modes have been widely used to monitor thin-film deposition for quite some time based on the inertia-frequency effects of the thin film on the QCRs, and are called quartz-crystal microbalances (QCMs) for thin-film and other applications, such as mass, chemical, and biological sensing. The effect of a thin film on a QCR is multifold, including thin-film mass density (inertia), elastic constant (stiffness), and thickness, etc. In the simplest description (the well-known Sauerbrey equation), the inertia of a thin film lowers the resonant frequencies of a QCR [1], [2]. This effect alone can be used to measure the product of the thin-film mass density and thickness. There have been more sophisticated 1-D models based on pure TSh modes depending on the plate thickness coordinate only, showing both the inertial and stiffness effects of the mass layer [3], [4]. These pure thickness mode models are valid for uniform films on unbounded plates only, without inplane variations in the plate. Behaviors of real devices are more complicated for several reasons and can deviate, sometimes considerably, from the results of pure thickness mode models. For example, due to the so-called energy-trapping phenomenon, the TSh vibration is not uniform and is mainly under the mass layer and decays exponentially away from the mass layer edge. There have been few attempts that consider the inplane variation of the TSh mode [5]–[7].

Recently, it has been pointed out [8] that the mass layer on a QCM is sometimes nonuniform and its effects are not well understood. Therefore, further research is needed in this direction. This paper is concerned with a nonuniform mass layer on a QCR. While there have been a few published results on nonuniform mass layers or nonuniform electrodes either for QCMs [9], [10] or energy trapping in resonator applications [11]–[14], these analyses are all for strip resonators with mode and mass layer (or electrode) thickness variations depending on only one inplane coordinate. For an accurate understanding of the effect of nonuniform mass layers in real devices, a more sophisticated analysis with the mass layer thickness and mode variations depending on the inplane coordinates of the resonator plate is necessary.

In this paper, we study the effect of the nonuniform thickness of a thin mass layer on a QCR with inplane variations in both directions. A theoretical analysis is performed using Mindlin's 2-D equation [15] for TSh vibrations of a quartz plate. An elliptical mass layer with stepped thickness is considered. The number of steps in the mass layer thickness variation is arbitrary. Therefore, the model can approximate a gradually varying mass layer thickness to any desired accuracy using a sufficiently large number of steps. An elliptic mass layer is chosen because it is known to be most compatible with the distribution of the TSh vibration and, therefore, it is optimal in the sense of [16] and [17]. Due to material anisotropy, an elliptical mass layer allows an exact analysis based on the plate equation while a circular mass layer does not.

II. Structure

For our purpose, it is sufficient to consider an unbounded plate of AT-cut quartz as shown in Fig. 1. The plate has a thickness $2h$ and a mass density ρ. There is a thin, elliptical mass layer with stepped thickness on the top of the crystal plate. The density of the mass layer is ρ'. Its varying thickness is $2h'$ which is piecewise constant between two neighboring ellipses. The mass layer is assumed to be very thin. Only its inertia will be considered. Its stiffness will be neglected [1], [2]. Consider the case of N ellipses. The Nth ellipse represents the boundary of the mass layer. Beginning from the center, the nth ellipse is described by

$$\frac{x_1^2}{\left(a^{(n)}\right)^2 \gamma_{11}/\gamma_{55}} + \frac{x_3^2}{\left(a^{(n)}\right)^2} = 1, \quad n = 1, 2, \ldots, N. \qquad (1)$$

Manuscript received June 24, 2010; accepted July 23, 2010. Date of publication September 27, 2010; date of current version February 09, 2011. The work was supported in part by the NSFC (Nos. 10832009 and 10725210) and in part by the National Basic Research Program of China (No. 2009CB623200). The associate editor coordinating the review of this paper and approving it for publication was Dr. Sandro Carrara.

N. Liu and J. Yang are with the Department of Engineering Mechanics, University of Nebraska, Lincoln, NE 68588-0526 USA.

W. Chen is with the Department of Engineering Mechanics, Zhejiang University, Hangzhou 310027, China (e-mail: chenwq@zju.edu.cn).

Digital Object Identifier 10.1109/JSEN.2010.2064297

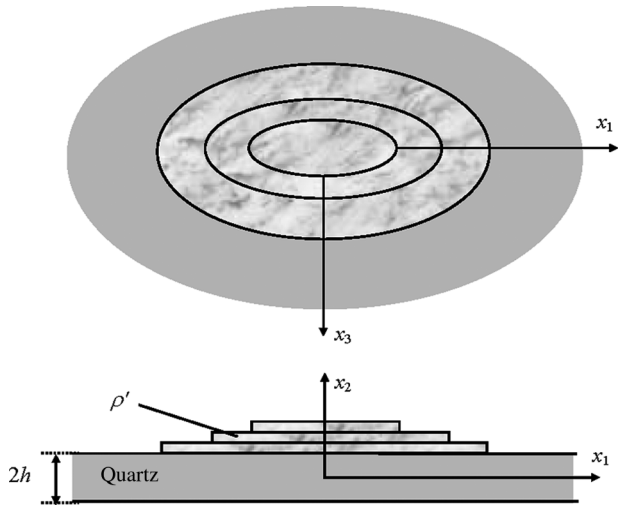

Fig. 1. Top and side views of a quartz plate with a nonuniform mass layer of stepped thickness.

The semimajor and semiminor axes are $a^{(n)}\sqrt{\gamma_{11}/\gamma_{55}}$ and $a^{(n)}$, respectively. We also denote $a^{(0)} = 0$ and $a^{(N+1)} = \infty$. For AT-cut quartz, $\gamma_{11} = 79.27$, and $\gamma_{55} = 49.90 \times 10^9$ N/m^2. The ratio between the major and minor axes is 1.26 which is very close to the optimal electrode shape determined in [16] and [17]. We need to analyze $N+1$ regions of $(a^{(n-1)}, a^{(n)})$ with $n = 1, 2, \ldots, N+1$. Quartz is a material with very weak piezoelectric coupling. For a frequency analysis, we will neglect the small coupling as usual.

III. Governing Equations

In general, TSh vibration may couple to flexural motion in a quartz plate. This coupling depends on the plate dimensions and is strong only for certain aspect ratios (length/thickness) of the plate [15]. For thin plates, the coupling to flexure is less likely to occur. For our purpose, we assume that the coupling to flexure has been avoided through design and we will consider pure TSh vibration with the following approximate displacement field [16]:

$$u_1(x_1, x_2, x_3, t) \cong x_2\psi_1(x_1, x_3, t), \quad u_2 \cong 0, \quad u_3 \cong 0 \quad (2)$$

where $\psi_1(x_1, x_3, t)$ is the plate TSh displacement. We consider free vibrations with a frequency ω which is to be determined. For the nth region, the governing equation for ψ_1 in [15]

$$\gamma_{11}\frac{\partial^2\psi_1}{\partial x_1^2} + \gamma_{55}\frac{\partial^2\psi_1}{\partial x_3^2} - 3h^{-2}\left(\kappa^{(n)}\right)^2 c_{66}\psi_1 + \left(1 + 3R^{(n)}\right)\rho\omega^2\psi_1 = 0 \quad (3)$$

where c_{pq} are the usual elastic stiffness constants, and

$$\left(\kappa^{(n)}\right)^2 = \frac{\pi^2}{12}\left(1 + R^{(n)}\right), \quad R^{(n)} = \frac{\rho' h'^{(n)}}{\rho h}, \quad (4)$$

$$\gamma_{11} = \frac{s_{33}}{s_{11}s_{33} - s_{13}^2}, \quad \gamma_{55} = \frac{1}{s_{55}}. \quad (5)$$

s_{pq} are the elastic compliances. From (3), we can determine the so-called cutoff frequency of the fundamental TSh mode independent of x_1 and x_3 as

$$\left(\omega_\infty^{(n)}\right)^2 = \frac{3\left(\kappa^{(n)}\right)^2 c_{66}}{\rho h^2\left(1 + 3R^{(n)}\right)} \cong \frac{\pi^2 c_{66}}{4h^2\rho}\left(1 - 2R^{(n)}\right) \quad (6)$$

where the approximation is for small $R^{(n)}$ and is not used in the remainder of this paper. Above the cutoff frequencies, the fields are oscillatory. Below the cutoff frequencies, the fields decay or grow. We consider the case when the mass layer is thicker in the middle as shown in Fig. 1 with

$$R^{(1)} > R^{(2)} > \ldots > R^{(N+1)} = 0. \quad (7)$$

We are interested in the so-called energy trapped modes for which the frequency ω is within the interval of

$$\omega_\infty^{(1)} < \omega < \omega_\infty^{(N+1)}. \quad (8)$$

In this frequency range, ψ_1 is oscillatory in the inner most central region under the mass layer and decays outside the mass layer. In an annular region of the mass layer, ψ_1 may be oscillatory or decaying depending on whether ω is above or below the cutoff frequency of the particular annular region.

IV. Free Vibration Solution

In the (x_1, x_3) plane, we introduce a new coordinate system (ξ_1, ξ_3) by

$$x_1 = \xi_1\sqrt{\gamma_{11}/\gamma_{55}}, \quad x_3 = \xi_3. \quad (9)$$

In this new coordinate system, the ellipses in (1) are transformed into circles described by

$$\frac{\xi_1^2}{\left(a^{(n)}\right)^2} + \frac{\xi_3^2}{\left(a^{(n)}\right)^2} = 1. \quad (10)$$

Equation (3) becomes

$$\frac{\partial^2\psi_1}{\partial\xi_1^2} + \frac{\partial^2\psi_1}{\partial\xi_3^2} - 3h^{-2}\left(\kappa^{(n)}\right)^2 c_{66}\gamma_{55}^{-1}\psi_1 + \left(1 + 3R^{(n)}\right)\rho\omega^2\gamma_{55}^{-1}\psi_1 = 0. \quad (11)$$

We then introduce a polar coordinate system (r, θ) defined by

$$\xi_3 = r\cos\theta, \quad \xi_1 = r\sin\theta. \quad (12)$$

We are only interested in modes that are independent of θ. Then, (11) becomes

$$\frac{\partial^2\psi_1}{\partial r^2} + \frac{1}{r}\frac{\partial\psi_1}{\partial r} + \left(\alpha^{(n)}\right)^2\psi_1 = 0 \quad (13)$$

where

$$\left(\alpha^{(n)}\right)^2 = \left(1 + 3R^{(n)}\right)\rho\gamma_{55}^{-1}\omega^2 - 3h^{-2}\left(\kappa^{(n)}\right)^2 c_{66}\gamma_{55}^{-1}. \quad (14)$$

To be specific, we consider the case when ω is within

$$\omega_\infty^{(1)} < \omega_\infty^{(2)} < \cdots < \omega_\infty^{(N)} < \omega < \omega_\infty^{(N+1)}. \tag{15}$$

In this case, the TSh motion is oscillatory everywhere under the film and decays outside the film. Other cases are possible and can be treated similarly. Under (15), for $n = 1, 2, 3, \ldots, N$, we have $\left(\alpha^{(n)}\right)^2 > 0$. For $n = N+1$, $\left(\alpha^{(N+1)}\right)^2 < 0$ and we denote $\left(\alpha^{(N+1)}\right)^2 = -\beta^2$. Then, in different regions, general solutions to (13) can be written as

$$\psi_1 = AJ_0\left(\alpha^{(1)} r\right), \quad 0 \le r < a^{(1)} \tag{16}$$

$$\psi_1 = B^{(n)} J_0\left(\alpha^{(n)} r\right) + C^{(n)} Y_0\left(\alpha^{(n)} r\right), \quad a^{(n)} < r < a^{(n+1)}, \quad n = 1, \cdots N-1, \tag{17}$$

$$\psi_1 = DK_0(\beta r), \quad a^{(N)} < r < \infty \tag{18}$$

where A, $B^{(n)}$, $C^{(n)}$, and D are undetermined constants. J_0 and Y_0 are the zero-order Bessel functions of the first and second kinds, respectively. They oscillate and decay according to $1/\sqrt{r}$ for large r. K_0 is the zero-order modified Bessel function of the second kind which decays exponentially at infinity.

At the interfaces between neighboring regions, we have the continuity of ψ_1 and its normal derivative [18]

$$AJ_0\left(\alpha^{(1)} a^{(1)}\right) = B^{(2)} J_0\left(\alpha^{(2)} a^{(1)}\right) + C^{(2)} Y_0\left(\alpha^{(2)} a^{(1)}\right), \tag{19}$$

$$A\alpha^{(1)} J_0'\left(\alpha^{(1)} a^{(1)}\right) = B^{(2)} \alpha^{(2)} J_0'\left(\alpha^{(2)} a^{(1)}\right) + C^{(2)} \alpha^{(2)} Y_0'\left(\alpha^{(2)} a^{(1)}\right), \tag{20}$$

$$B^{(n)} J_0\left(\alpha^{(n)} a^{(n)}\right) + C^{(n)} Y_0\left(\alpha^{(n)} a^{(n)}\right) = B^{(n+1)} J_0\left(\alpha^{(n+1)} a^{(n)}\right) + C^{(n+1)} Y_0\left(\alpha^{(n+1)} a^{(n)}\right), \quad n = 2, 3, \ldots, N-1, \tag{21}$$

$$B^{(n)} \alpha^{(n)} J_0'\left(\alpha^{(n)} a^{(n)}\right) + C^{(n)} \alpha^{(n)} Y_0'\left(\alpha^{(n)} a^{(n)}\right) = B^{(n+1)} \alpha^{(n+1)} J_0'\left(\alpha^{(n+1)} a^{(n)}\right) + C^{(n+1)} \alpha^{(n+1)} Y_0'\left(\alpha^{(n+1)} a^{(n)}\right), \quad n = 2, 3, \ldots, N-1, \tag{22}$$

$$B^{(N)} J_0\left(\alpha^{(N)} a^{(N)}\right) + C^{(N)} Y_0\left(\alpha^{(N)} a^{(N)}\right) = DK_0\left(\beta a^{(N)}\right), \tag{23}$$

$$B^{(N)} \alpha^{(N)} J_0'\left(\alpha^{(N)} a^{(N)}\right) + C^{(N)} \alpha^{(N)} Y_0'\left(\alpha^{(N)} a^{(N)}\right) = D\beta K_0'\left(\beta a^{(N)}\right) \tag{24}$$

where a prime represents the differentiation with respect to the entire argument $\alpha^{(n)} r$ or βr. Equations (19)–(24) represent $2N$ linear homogeneous equations for A and $B^{(n)}$, $C^{(n)}$, and D. For nontrivial solutions of the undetermined constants, the determinant of the coefficient matrix must vanish, which gives the frequency equation that determines the resonant frequency ω. This will be performed numerically on a computer. The following identities are used to simplify the numerical calculation:

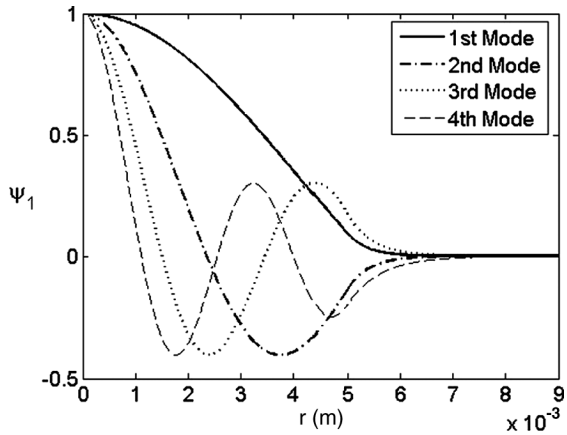

Fig. 2. Trapped modes for Case 1), uniform film $a = 5$ mm and $R = 2.5\%$.

$$J_0' = -J_1, \quad Y_0 = -Y_1, \quad I_0' = I_1, \quad K_0' = -K_1 \tag{25}$$

where I_0 is the zero-order modified Bessel function of the first kind which is needed when ω is in a different range than (15).

V. Numerical Results

As a numerical example, we consider an AT-cut quartz plate with a typical resonator thickness of $2h = 0.2$ mm. To examine the effects of the mass-layer thickness variation, we calculate three examples and compare the results. Case 1) is a plate with a uniform mass layer. Case 2) is for a plate with a mass layer whose thickness has one sudden change (step). Case 3) is similar to Case 2), with one sudden change in the thickness with a different amount. The specific parameters of the three cases are as follows.

1) Uniform film $a = 5$ mm, $R = 2.5\%$. The cutoff frequencies of the central and outer regions are 8 078 497 Hz and 8 273 188 Hz.
2) Relatively weakly nonuniform film: $a^{(1)} = 2.5$ mm, $R^{(1)} = 3\%$, $a^{(2)} = 5$ mm, $R^{(2)} = 2.5\%$. From the central to the outer regions, the cutoff frequencies are 8 042 263 Hz, 8 078 497 Hz, and 8 273 188 Hz.
3) Relatively strongly nonuniform film: $a^{(1)} = 2.5$ mm, $R^{(1)} = 4\%$, $a^{(2)} = 5$ mm, $R^{(2)} = 2.5\%$. The cutoff frequencies are 7 972 243 Hz, 8 078 497 Hz, and 8 273 188 Hz. The only difference between Cases 2) and 3) is $R^{(1)}$.

The frequencies and mode shapes of the trapped modes for the three cases are shown in Figs. 2–4, respectively. These modes are essentially under the mass layer (energy trapping). The modes are normalized by their maxima.

In Fig. 2 for Case 1), there are four trapped modes. They are all oscillatory under the film and decay outside it. The four modes are with zero, one, two, and three nodal points and slowly increasing frequencies. Ideally, only the first mode without nodal points is needed for mass sensing. The frequencies of the

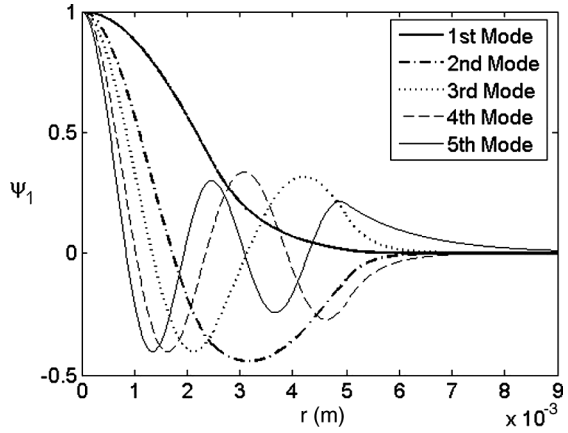

Fig. 3. Trapped modes for Case 2), nonuniform film $a^{(1)} = 2.5$ mm, $R^{(1)} = 3\%$, $a^{(2)} = 5$ mm, $R^{(2)} = 2.5\%$.

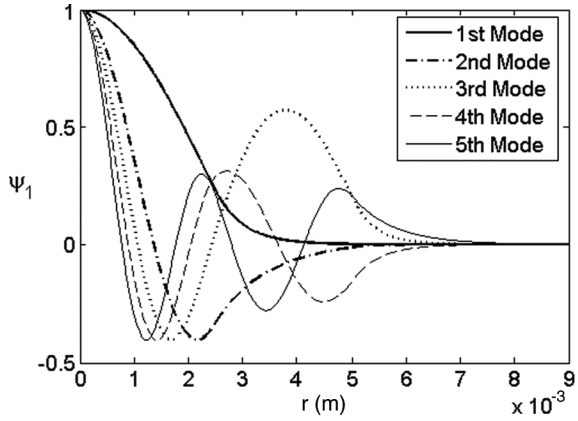

Fig. 4. Trapped modes for Case 3): nonuniform film $a^{(1)} = 2.5$ mm, $R^{(1)} = 4\%$, $a^{(2)} = 5$ mm, $R^{(2)} = 2.5\%$.

four modes are 8 083 967 Hz, 8 107 198 Hz, 8 148 456 Hz, and 8 206 412 Hz, respectively. They are slowly increasing.

In Fig. 3 for Case 2), five trapped modes are found. They can be classified into two categories. The first mode without a nodal point alone represents one category. It is oscillatory under the central circular region $r < a^{(1)}$ where the film is thick, and decays in both the annular region $a^{(1)} < r < a^{(2)}$ where the film is thin and the outer region $a^{(2)} < r$ where there is no film. The four other modes with one, two, three, and four nodal points are all oscillatory under the film everywhere $(r < a^{(2)})$ regardless of whether the film is thin or thick, and decay outside the film. The frequencies of the modes are 8 055 622 Hz, 8 095 289 Hz, 8 130 593 Hz, 8 191 140 Hz, and 8 260 625 Hz, respectively. The first three frequencies are slightly lower than those in Case 1) because of the additional mass of the thick central layer.

In Fig. 4, for Case (3), five trapped modes are found. They also fall into two categories. The first two modes with zero and one nodal point are oscillatory under the central circular region $r < a^{(1)}$ and decay outside it. The three other modes with two, three, and four nodal points are oscillatory everywhere under the film when $r < a^{(2)}$ and decay outside the film. The frequencies of the modes are 7 989 122 Hz, 8 055 574 Hz, 8 108 798 Hz, 8 164 732 Hz, and 8 229 204 Hz, respectively.

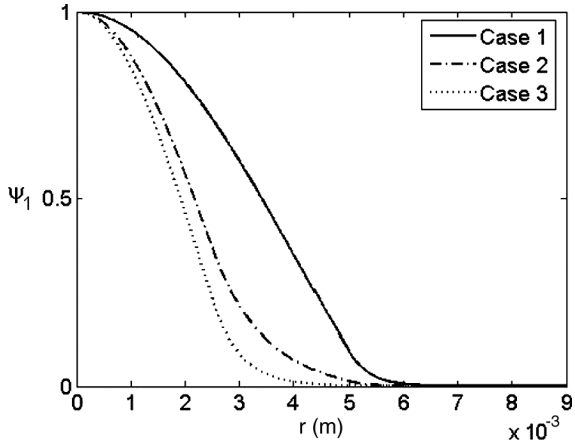

Fig. 5. First mode from Cases 1)–3).

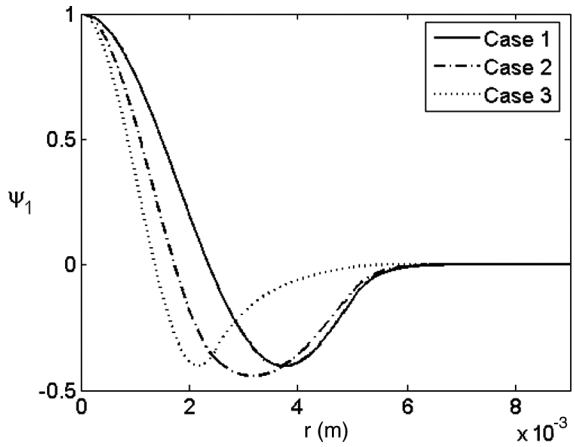

Fig. 6. Second mode from Cases 1)–3).

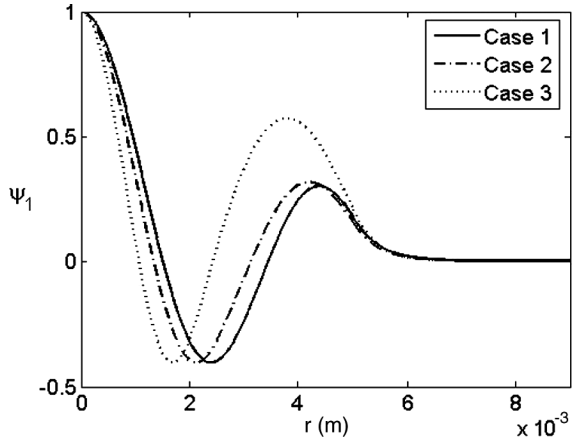

Fig. 7. Third mode from Cases 1)–3).

In Figs. 5–8, we plot the same mode from different cases in the same figure. Clearly, as the center of the film becomes thicker, the same mode is pushed toward the center.

VI. Conclusion

A nonuniform mass layer thicker at the center tends to confine more modes with nodal points under the mass layer and pushes the modes toward the center. In the region where the

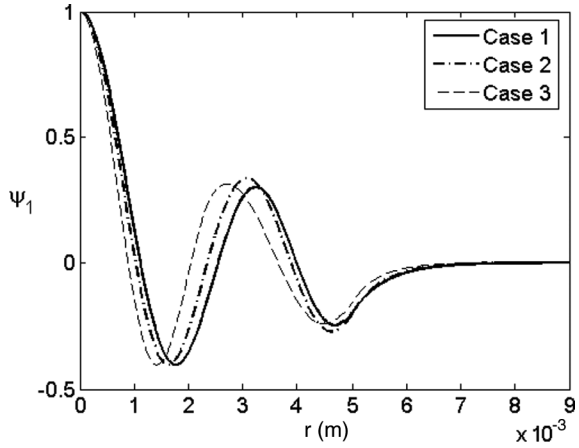

Fig. 8. Fourth mode from Cases 1)–3).

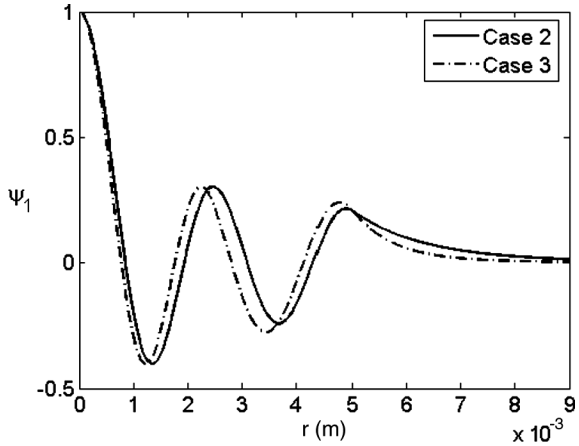

Fig. 9. Fifth mode from Cases 2) and 3).

film is thin, the vibration may be reduced significantly from oscillatory to decaying. The frequencies of the modes are slightly lowered when the film becomes thicker in the center. These effects cause considerable complications in mass sensing. (For a general discussion, the reader is referred to [8].) They also have implications in the actual operation of electrically forced vibrations of a QCR. If a trapped mode with a nodal point is pushed under the driving electrodes, the change of sign of the shear deformation across the nodal point causes charge cancellation on the electrodes and affects the impedance of the device.

REFERENCES

[1] A. Ballato and T. J. Lukaszek, "Mass-loading of thickness-excited crystal resonators having arbitrary piezo-coupling," *IEEE Trans. Sonics Ultrason.*, vol. SU-21, no. 4, pp. 269–274, Oct. 1974.

[2] J. A. Kosinski, "Thickness vibration of flat piezoelectric plates with massy electrodes of unequal thickness," in *Proc. IEEE Ultrasonics Symp.*, 2003, pp. 70–73.

[3] J. G. Miller and D. J. Bolef, "Acoustic wave analysis of the operation of quartz-crystal film-thickness monitors," *J. Appl Phys.*, vol. 39, no. 12, pp. 5815–5816, 1968.

[4] F. Boersma and E. C. van Ballegooyen, "Rotated Y-cut quartz crystal with two different electrodes treated as a one-dimensional acoustic composite resonator," *J. Acoust. Soc. Amer.*, vol. 62, no. 2, pp. 335–340, 1977.

[5] P. J. Cumpson and M. P. Seah, "The quartz crystal microbalances; radial/polar dependence of mass sensitivity both on and off the electrodes," *Meas. Sci. Technol.*, vol. 1, no. 7, pp. 544–555, 1990.

[6] F. Josse and Y. Lee, "Analysis of the radial dependence of mass sensitivity of modified electrode quartz crystal resonators," *Anal. Chem.*, vol. 70, no. 2, pp. 237–247, 1998.

[7] B. A. Martin and H. E. Hager, "Velocity profile on quartz crystals oscillating in liquids," *J. Appl. Phys.*, vol. 65, no. 7, pp. 2630–2635, 1989.

[8] J. R. Vig and A. Ballato, "Comments about the effects of nonuniform mass loading on a quartz crystal microbalance," *IEEE Trans. Ultrason., Ferroelect., Freq. Control*, vol. 45, no. 5, pp. 1123–1124, Sep. 1998.

[9] C. van der Steen, F. Boersma, and E. C. van Ballegooyen, "The influence of mass loading outside the electrode area on the resonant frequencies of a quartz-crystal microbalance," *J. Appl. Phys.*, vol. 48, no. 8, pp. 3201–3205, 1977.

[10] E. C. van Ballegooyen, F. Boersma, and C. van der Steen, "Influence of the thickness of tabs on the resonating properties of a quartz crystal," *J. Acoust. Soc. Amer.*, vol. 62, no. 5, pp. 1189–1195, 1977.

[11] J. S. Yang, H. Xue, H. Y. Fang, Y. T. Hu, J. Wang, and L. J. Shen, "Effects of electrodes with varying thickness on energy trapping in thickness-shear quartz resonators," *IEEE Trans. Ultrason., Ferroelect., Freq. Control*, vol. 54, no. 4, pp. 892–895, Apr. 2007.

[12] J. Wang, L. J. Shen, and J. S. Yang, "Effects of electrodes with continuously varying thickness on energy trapping in thickness-shear mode quartz resonators," *Ultrason.*, vol. 48, no. 2, pp. 150–154, 2008.

[13] J. S. Yang, Z. G. Chen, and H. P. Hu, "Electrically forced vibration of a thickness-twist mode piezoelectric resonator with non-uniform electrodes," *Acta Mechanica Solida Sinica*, vol. 20, no. 3, pp. 266–274, 2007.

[14] J. S. Yang, Z. G. Chen, and Y. T. Hu, "Vibration of a thickness-twist mode piezoelectric resonator with asymmetric, non-uniform electrodes," *IEEE Trans. Ultrason., Ferroelect., Freq. Control*, vol. 55, no. 4, pp. 841–848, Apr. 2008.

[15] R. D. Mindlin and W. J. Spencer, "Anharmonic, thickness-twist overtones of thickness-shear and flexural vibrations of rectangular, AT-cut quartz plates," *J. Acoust. Soc. Amer.*, vol. 42, no. 6, pp. 1268–1277, 1967.

[16] R. D. Mindlin, "Optimal sizes and shapes of electrodes for quartz resonators," *J. Acoust. Soc. Amer.*, vol. 43, no. 6, pp. 1329–1331, 1968.

[17] Z. T. Yang and J. S. Yang, "Optimal electrode shape and size of a few singly rotated quartz and langasite resonators," *IEEE Trans. Ultrason., Ferroelect., Freq. Control*, vol. 56, no. 2, pp. 237–238, Feb. 2009.

[18] H. F. Tiersten, *Linear Piezoelectric Plate Vibrations*. New York: Plenum, 1969.

Nan Liu, photograph and biography not available at the time of publication.

Jiashi Yang, photograph and biography not available at the time of publication.

Weiqiu Chen, photograph and biography not available at the time of publication.